The reverse TCA cycle and reductive amino acid synthesis pathways contribute to electron balance in a *Rhodospirillum rubrum* Calvin cycle mutant

Alexandra L. McCully[1,2†], Maureen C. Onyeziri[1†], Breah LaSarre[1], Jennifer R. Gliessman[1], and James B. McKinlay[1]*

[1]Department of Biology, Indiana University, Bloomington, IN

[2] Current address: Department of Civil and Environmental Engineering, Stanford University, CA

[†]Equal contributions.

*Corresponding author, jmckinla@indiana.edu

Abstract

Purple nonsulfur bacteria (PNSB) use light for energy and organic substrates for carbon and electrons when growing photoheterotrophically. This lifestyle generates more reduced electron carriers than are required for biosynthesis. It is essential that this excess reducing power be oxidized for photoheterotrophic growth to occur. Diverse PNSB commonly rely on the CO_2-fixing Calvin cycle to oxidize excess reducing power. Some PNSB additionally utilize H_2 production or reduction of electron acceptors, such as dimethylsulfoxide, as alternative reductive pathways to the Calvin cycle. *Rhodospirillum rubrum* Calvin cycle mutants defy this trend by growing phototrophically on relatively oxidized substrates like malate and fumarate without H_2 production or access to electron acceptors. How *Rs. rubrum* Calvin cycle mutants maintain electron balance under these conditions was unknown. Here, using ^{13}C-tracer experiments and physiological assays, we found that *Rs. rubrum* Calvin cycle mutants use a reductive arm of the tricarboxylic acid cycle when growing phototrophically on malate and fumarate. The reductive

synthesis of amino acids stemming from α-ketoglutarate is also likely important for electron balance, as supplementing the growth medium with α-ketoglutarate-derived amino acids prevented *Rs. rubrum* Calvin cycle mutant growth unless dimethylsulfoxide was provided as an electron acceptor. Fluxes estimated from ^{13}C-tracer experiments also suggested the preferential use of a reductive isoleucine synthesis pathway when the Calvin cycle was genetically inactivated; however, this pathway was not essential for growth of a Calvin cycle mutant.

Importance. The lifestyle by which PNSB use organic carbon and light for energy comes with a challenge in managing electrons. Excess electrons from the organic substrates can be coupled to the assimilation of CO_2 in the Calvin cycle, avoiding a buildup of reduced electron carriers that would halt metabolism. As an exception, *Rs. rubrum* can grow without the Calvin cycle when provided with light and relatively oxidized substrates. By tracking stable isotopes in a *Rs. rubrum* Calvin cycle mutant, we observed the reversal of an arm of the tricarboxylic acid cycle, feeding electron-requiring amino acid synthesis pathways. Providing the mutant with these amino acids prevented growth, suggesting that their synthesis is required for electron balance. Our results highlight the contribution of biosynthetic reactions to electron balance and the metabolic diversity that exists between PNSB, as most PNSB cannot grow without the Calvin cycle under the conditions used in this study.

Introduction

Purple nonsulfur bacteria (PNSB) are a metabolically versatile group that are often cultured under anaerobic conditions supporting photoheterotrophic growth, wherein light is used for energy and organic compounds are used for carbon and electrons. This lifestyle presents a

47 challenge in maintaining electron balance, as oxidative metabolic pathways generate an excess of
48 reduced electron carriers, or reducing power (1, 2). Oxidation of excess reducing power is
49 essential for growth and is often coupled to CO_2 fixation in the Calvin cycle. Calvin cycle
50 mutants are generally incapable of photoheterotrophic growth unless another means of electron
51 disposal is possible, such as reduction of electron acceptors, like dimethylsulfoxide (DMSO) (3-
52 6), or H_2 production via nitrogenase (7-11). Such trends have been observed for several model
53 PNSB including *Rhodobacter sphaeroides* (3, 4, 6, 11), *Rhodobacter capsulatus* (5, 12), and
54 *Rhodopseudomonas palustris* (7-10). An exception to this general observation is *Rhodosprillum*
55 *rubrum,* for which mutants incapable of Calvin cycle activity can grow photoheterotrophically
56 on relatively oxidized substrates, like malate and fumarate, without access to electron acceptors
57 and without producing H_2 (8, 13). However, these alternative electron-balancing mechanisms
58 were still required by *Rs. rubrum* Calvin cycle mutants for photoheterotrophic growth on more
59 reduced substrates, like succinate (8). The mechanism by which *Rs. rubrum* Calvin cycle mutants
60 maintain electron balance is unknown, but the fact that growth only occurs on relatively oxidized
61 substrates suggests that there is a constraint on the number of excess electrons that can be dealt
62 with in these mutants.
63
64 Alternative central metabolic pathways that could maintain electron balance during phototrophic
65 growth in the absence of the Calvin cycle have been explored in silico (14), and some have been
66 ruled out. For example, phototrophic growth by Calvin cycle mutants on malate could be
67 possible if the cells produced formate (14). However, we previously found that *Rs. rubrum*
68 Calvin cycle mutants did not excrete formate, nor did they accumulate polyhydroxybutyrate, an
69 electron rich storage polymer that could potentially help maintain electron balance (8). There is

70 also evidence that an alternative CO_2-fixing pathway could be involved, given that an *Rs. rubrum*
71 Calvin cycle mutant was observed to grow when CO_2 was the sole carbon source (15). The CO_2-
72 fixing ethylmalonyl-CoA pathway can substitute for the Calvin cycle to achieve electron balance
73 during phototrophic growth on acetate (16). However, during phototrophic growth on malate, the
74 ethylmalonyl-CoA pathway would not satisfy electron balance given that more reducing power
75 would be made enroute to the ethylmalonyl-CoA pathway than could subsequently be oxidized
76 by the ethylmalonyl-CoA pathway (14). Another CO_2-fixing pathway that might participate in
77 electron balance in *Rs. rubrum* Calvin cycle mutants is the reverse TCA cycle (14, 17).
78
79 Here we used ^{13}C-tracer experiments to gain insight into electron-balancing mechanisms in a *Rs.*
80 *rubrum* Calvin cycle mutant. Labeling patterns suggested the involvement of a reductive arm of
81 the TCA cycle from fumarate to α-ketoglutarate (αKG). This pathway feeds into reductive
82 pathways for the synthesis of αKG-derived amino acids. These amino acid synthesis pathways
83 also likely contribute to electron balance, as adding αKG-derived amino acids to the medium
84 prevented photoheterotrophic growth of a Calvin cycle mutant on malate unless DMSO was
85 added as an electron acceptor. Flux estimates from labeling experiments also revealed the
86 preferential use of a reductive isoleucine synthesis pathway over an alternative pathway in the
87 Calvin cycle mutant. Thus, *Rs. rubrum* appears to have flexibility within its innate biosynthetic
88 pathways to satisfy electron balance during phototrophic growth on relatively oxidized
89 substrates.

Results and Discussion

^{13}C-metabolic flux analysis of *Rs. rubrum* strains. To gain insight into how *Rs. rubrum* maintains electron balance without the Calvin cycle during phototrophic growth on relatively oxidized substrates, we performed ^{13}C-metabolic flux analysis (^{13}C-MFA) to estimate in vivo metabolic fluxes. In ^{13}C-MFA, the activities of different pathways generate signature patterns of ^{12}C and ^{13}C that are imprinted on proteinaceous amino acids, which can be deciphered using gas chromatography-mass spectrometry (GC-MS) (18). Software is then used to identify a set of fluxes that can explain the observed labeling patterns. Directly measured fluxes, such as those for excreted products and those needed to generate a defined biomass composition, are also taken into account. We grew wild-type (WT) *Rs. rubrum* and a Calvin cycle mutant lacking genes for phosphoribulokinase (PRK) and ribulose-1,5-bisphosphate carboxylase (RuBisCO), hereon referred to as the ΔCalvin mutant, each in a defined medium with [1,4-^{13}C]fumarate. Cells were harvested in exponential phase to determine mass isotopomer distributions (MIDs) in proteinaceous amino acids (i.e., labeling patterns). No H_2 was detected at the time of harvesting, indicating that H_2 production was not involved in electron balance. High performance liquid chromatography (HPLC) analysis of culture supernatants revealed that malate was excreted by each strain but more so by the ΔCalvin mutant (malate yield [mol/100 mol fumarate] ± SD: WT, 8.5 ± 3.9; ΔCalvin, 46.2 ± 24.9).

We then used the ^{13}C-MFA software 13CFLUX2 (19) to estimate a set of fluxes that could explain the observed amino acid MIDs (Table S1), malate excretion, and the *Rs. rubrum* biomass composition (Table S2). For the *Rs. rubrum* biomass composition we determined the protein content (75 ± 4% of dry cell weight [DCW]; Fig. S1) and amino acid composition (Table

S3), and assumed that the remaining composition was similar to that of *Rp. palustris* (10). Fitting algorithms used in ^{13}C-MFA can potentially generate multiple solutions. The fitting algorithm is automatically constrained for carbon balance but does not account for electron balance. Thus, one way to determine if an optimal solution is realistic is to examine whether it satisfies electron balance; the total flux through reductive reactions must equal the total flux through oxidative reactions. Neither flux map fully satisfied electron balance, but the violation for the ΔCalvin mutant flux map was severe (Fig. S2); optimal solutions suggested that WT reductive fluxes ($NAD(P)^+$ generating) countered 86% of the oxidative fluxes (NAD(P)H generating) whereas ΔCalvin reductive fluxes countered only 56% of the oxidative fluxes. We therefore made a redox-constrained model wherein the sum of fluxes through reductive reactions must equal the fluxes through oxidative reactions. The optimal solutions from the redox-constrained models (Fig. 1, Table S4) identified a set of fluxes that could still explained the observed MIDs for both strains (Fig. 2A). However, like the flux solutions for the unconstrained models (Table S4), the optimal flux solutions were also unable to fully satisfy the expected fluxes to biomass and excreted malate for both strains (Fig. S3). Given this disagreement between simulated and experimental biomass fluxes and the need to introduce a redox constraint, we do not place high confidence in the resulting flux values. Nevertheless, the resulting optimal solutions point to qualitative trends that could contribute to electron balance, which we address below.

Reverse TCA cycle flux from α-ketoglutarate to fumarate in *Rs. rubrum*. Comparing the flux maps between WT *Rs. rubrum* and the ΔCalvin mutant revealed lower gluconeogenic (GNG) flux in the mutant due to the combination of higher malate excretion and the absence of Calvin cycle activity. Also of note was bifurcated TCA cycle flux converging on αKG for both strains

(Fig. 1). The reverse TCA cycle had previously been proposed as a mechanism by which a Calvin cycle mutant could achieve electron balance (14) based on αKG synthase activity detected in *Rs. rubrum* cell extracts (17). Thus, despite the estimated small magnitude of the flux from fumarate to αKG (< 1 mole % of the fumarate uptake rate) we questioned whether this reverse TCA cycle flux could be important for electron balance.

We first wanted to verify that the reverse TCA cycle flux from fumarate to αKG was associated with at least one signature labeling pattern; in other words, we asked what labeling patterns would be generated by reverse TCA cycle activity. We noticed that higher proportions of double and triple-labeled glutamate (Glu) were observed in the ΔCalvin mutant compared to WT *Rs. rubrum* (Fig. 2). We reasoned that in the case of reverse TCA cycle flux from [1,4-^{13}C]fumarate to αKG, triple-labeled Glu could be generated when $^{13}CO_2$, liberated from decarboxylation reactions in the catabolism of [1,4-^{13}C]fumarate, would carboxylate [1,4-^{13}C]succinyl-CoA to form triple-labeled αKG, from which Glu is derived (Fig. 3A). Double-labeled Glu can be explained by unlabeled CO_2 participating in the same carboxylation of succinyl-CoA (Fig. 3B). The sources of unlabeled CO_2 could include catabolism of unlabeled fumarate carried over from the starter culture or repeated turns of the oxidative TCA cycle, which would eventually generate unlabeled CO_2 even from [1,4-^{13}C]fumarate (Fig. 3B).

To confirm that higher molecular weight (MW) Glu isotopomers were a signature of reverse TCA cycle flux, we ran fitting algorithms using a model in which TCA cycle flux was constrained to be strictly forward, or oxidative, with no reverse flux. Indeed, using this model with strictly forward TCA cycle for the ΔCalvin mutant resulted in a disagreement between

159 simulated and observed Glu labeling patterns (Fig. 2). However, the WT optimal solutions from
160 this model could explain the Glu labeling patterns (Fig. 2). Enrichment of higher MW amino
161 acid isotopomers was a signature of Calvin cycle activity in our previous ^{13}C-labeling studies
162 with *Rp. palustris* (9, 10). Thus, in a WT model constrained to have only forward TCA cycle
163 flux, the higher MW Glu isotopomers could still be explained from Calvin cycle activity. In the
164 ΔCalvin mutant, reverse TCA cycle activity is the only pathway that can generate high MW Glu
165 isotopomers, explaining the discrepancy between simulated and observed Glu MIDs when the
166 TCA cycle was constrained to the forward direction.
167
168 MIDs from a separate labeling experiment, wherein WT and ΔCalvin *Rs. rubrum* strains were
169 cultured with unlabeled malate and $NaH^{13}CO_3$ as a source of $^{13}CO_2$, also suggested reverse TCA
170 cycle flux from fumarate to αKG for both strains. In this case, the reverse TCA cycle flux was
171 determined with greater confidence for the ΔCalvin mutant at ~ 3 ± 1 mole % of the fumarate
172 uptake rate (Fig. 4A). The standard deviation for this activity in the WT strain remained large
173 (Fig. 4A), likely due to the possibility that the signature high MW Glu MIDs can also be
174 generated by the Calvin cycle. Consistent with the previous labeling experiment, the ΔCalvin
175 mutant also exhibited a higher proportion of higher MW Glu isotopomers compared to the WT
176 strain (Fig. 4B). Even though both the reverse TCA cycle and the Calvin cycle can generate
177 higher MW Glu isotopomers, labeling patterns generated by the Calvin cycle are more likely to
178 influence amino acids derived from glycolytic intermediates than from TCA cycle intermediates
179 like αKG, from which Glu is derived. αKG labeling is expected to be more heavily influenced by
180 the direct uptake of fumarate or malate nearby in the TCA cycle (9, 10). Thus the consistently
181 elevated proportions of high MW Glu isotopomers in the ΔCalvin mutant support the notion that

182 the labeling patterns were generated nearby and likely in response to the absence of the Calvin
183 cycle.
184
185 **The *Rs. rubrum* gene annotated to encode αKG synthase is not required to generate higher**
186 **MW Glu isotopomers.** We sought to genetically verify the involvement of the reverse TCA
187 cycle in maintaining electron balance in *Rs. rubrum*. The *Rs. rubrum* gene Rru_A2721 is
188 annotated to encode the αKG synthase α-subunit, an enzyme normally required for reverse TCA
189 cycle flux. We deleted Rru_A2721 in WT *Rs. rubrum* and in a ΔPRK mutant, which lacks the
190 gene for the essential Calvin cycle enzyme phosphoribulokinase (PRK). The ΔPRK mutant
191 cannot fix CO_2 via the Calvin cycle, has similar growth trends to the ΔCalvin mutant (8), and
192 offered a convenient background for genetic engineering because, unlike the ΔCalvin mutant, it
193 is not resistant to the antibiotic needed to select for integration of the suicide vector. We then
194 examined whether ΔRru_A2721 mutants generated high MW Glu under ^{13}C-labeling conditions
195 permitting growth. Specifically, we compared amino acid MIDs from WT *Rs. rubrum* to those
196 from a ΔRru_A2721 mutant grown with [1,4-^{13}C]succinate, and we also compared patterns from
197 the ΔPRK mutant and the ΔPRK ΔRru_A2721 mutant grown with [1,4-^{13}C]succinate and DMSO
198 as an alternative electron acceptor to permit growth. Both strains with the ΔRru_A2721 mutation
199 produced high MW Glu, including triple-labeled Glu (Table S1). There are three possibilities
200 that could explain this observation: (i) Rru_A2721 does not encode αKG synthase; (ii) *Rs.*
201 *rubrum* has redundant αKG synthase activities; or (iii) in the case of the mutants lacking PRK,
202 the high MW Glu patterns are generated by an activity other than the reverse TCA cycle or the
203 Calvin cycle.
204

In considering other pathways that might generate high MW Glu isotopomers, the ethylmalonyl-CoA pathway was already ruled out because (i) it would not achieve electron balance during growth on malate (14) and (ii) our optimal flux solutions showed negligible flux through the ethylmalonyl-CoA pathway (Table S4). We also considered the involvement of CO dehydrogenase, which was previously found to be upregulated in an H_2-producing *Rs. rubrum* Calvin cycle mutant (20). The authors speculated that CO dehydrogenase could contribute to electron balance by operating in reverse of the normally ascribed physiological direction, reducing CO_2 to CO with subsequent coupling of CO oxidation to H_2 production (20). However, we did not observe H_2 accumulation in our experiments nor would such a scenario explain the high MW Glu isotopomers. In acetogens, CO dehydrogenase can participate in the conversion of CO_2 to acetyl-CoA via the Wood-Ljungdahl pathway (21). This activity could contribute to label enrichment but the *Rs. rubrum* CO dehydrogenase is thought to be incapable of such activity (22). In agreement with this notion, including a reaction converting 2 CO_2 into AcCoA in a flux model unconstrained for electron balance and lacking the Calvin cycle resulted in solutions that favored cleavage of AcCoA into 2 CO_2 rather than the creation of AcCoA from CO_2 (Table S4). These solutions also preserved reverse TCA cycle flux from fumarate to αKG. Thus, although the possibility of another unknown reductive pathway in *Rs. rubrum* cannot be ruled out, the labeling patterns we have observed thus far point to the activity of reverse TCA cycle flux from fumarate to αKG.

An *Rp. palustris* Calvin cycle mutant does not generate higher MW Glu isotopomers. *Rs. rubrum* Calvin cycle mutants can grow on fumarate and malate, whereas *Rp. palustris* Calvin cycle mutants cannot unless they can dispose of excess electrons as H_2 (8). We therefore used

this knowledge to test the hypothesis that the increased proportion of high MW Glu isotopmers in the *Rs. rubrum* ΔCalvin mutant is indicative of an electron-balancing mechanism that *Rs. rubrum* possesses but *Rp. palustris* does not. To test this notion, we performed four separate labeling experiments with the H_2-producing NifA* *Rp. palustris* strain CGA676 and its ΔCalvin mutant counterpart, CGA4011 (8), using [1,4-^{13}C]succinate, [1,4-^{13}C]fumarate, unlabeled succinate with $NaH^{13}CO_3$, or unlabeled malate with $NaH^{13}CO_3$. Unlike the *Rs. rubrum* ΔCalvin mutant, which showed a higher abundance of higher MW Glu than the WT strain, the *Rp. palustris* ΔCalvin mutant showed a lower abundance of higher MW Glu compared to the parent NifA* strain in all labeling experiments (Fig. 5). Thus, the higher MW Glu isotopomers observed in the *Rs. rubrum* ΔCalvin mutant arose as the result of a pathway that distinguishes *Rs. rubrum* from *Rp. palustris*, with reverse TCA cycle flux from fumarate to αKG as the likely candidate.

αKG-derived amino acids inhibit growth of a *Rs. rubrum* Calvin cycle mutant. Similar to our findings for photoheterotrophic growth in *Rp. palustris* (9, 10), the small amount of flux to αKG in our *Rs. rubrum* flux maps suggests that the magnitude of the flux to αKG is primarily dictated by the need for αKG as a biosynthetic precursor. αKG is a precursor for the amino acids Glu, Gln, Pro, and Arg, all of which are produced via reductive pathways and thus could also contribute to electron balance (Fig. 1C and 6A). Glu, Gln, Pro, and Arg are all inhibitors of their own synthesis pathways in *E. coli* (23-27). We predicted that if these amino acid synthesis pathways are similarly regulated in *Rs. rubrum* then their synthesis could be repressed by supplementing the growth medium with these amino acids; in this manner, supplementation with these amino acids might avert the reverse TCA cycle flux to αKG. The addition of all four amino

acids (EQPR) had no effect on WT *Rs. rubrum* phototrophic growth trends on malate but prevented ΔCalvin mutant culture growth (Fig. 6B). These results could be interpreted to mean that adding Glu, Gln, Pro, and Arg inhibited the respective amino acid synthesis pathways and thereby prevented electron balance. An alternative explanation could be that, even at 0.2 mM each, the catabolism of these amino acids could contribute to an excess of reducing power. However, adding four amino acids derived from oxaloacetate (DTMK) did not affect the growth of either the WT or the ΔCalvin mutant on malate (Fig. 6C). The addition of either 0.7 mM isoleucine (Fig. 7) or 0.7 mM leucine (data not shown), both of which should also generate reducing power through their catabolism, also failed to affect the growth of the ΔCalvin mutant on malate. While these results do not rule out the possibility of the catabolism of Glu, Gln, Pro, and Arg creating an electron imbalance, they show that the inhibitory effect of Glu, Gln, Pro, and Arg on the ΔCalvin mutant was specific to this mixture. To verify that the growth inhibition caused by the αKG-derived amino acids was linked to electron balance rather than an unrelated form of toxicity, we repeated the growth experiment in medium supplemented with the electron acceptor DMSO. Indeed, adding DMSO rescued ΔCalvin mutant growth on malate in the presence of αKG-derived amino acids (Fig. 6D). Thus, the addition of Glu, Gln, Pro, and Arg created a growth-inhibiting electron imbalance in the ΔCalvin mutant.

Since the production of αKG-derived amino acids appears to contribute to electron balance, one could expect the ΔCalvin mutant to generate more of these amino acids. However, we did not observe a shift in biomass composition to favor the production of αKG-derived amino acids in the ΔCalvin mutant. Whole cell protein content and amino acid composition were similar between WT *Rs. rubrum* and the ΔCalvin mutant (Fig. S1 and Table S3). Excretion of

these amino acids is also unlikely because (i) accumulation of αKG-derived amino acids represses growth of the ΔCalvin mutant (Fig. 6B) and (ii) excretion would leave electron disposal unconstrained and would thus allow for the ΔCalvin mutant to achieve electron balance during phototrophic growth on succinate, which is not observed (8). Thus, the contribution of the combined reverse TCA cycle flux and synthesis of Glu, Gln, Pro, and Arg to electron balance is likely limited by the constraints of the *Rs. rubrum* biomass composition.

Isoleucine is produced exclusively by a reductive pathway in the *Rs. rubrum* ΔCalvin mutant. *Rs. rubrum* has two pathways for isoleucine synthesis. One pathway uses 1 oxaloacetate and 1 pyruvate, and the other uses 1 AcCoA and 2 pyruvate (Fig. 7A). While both pathways are technically reductive, we herein consider the AcCoA-utilizing pathway to be oxidative because the path from fumarate to 2 pyruvate + 1 AcCoA generates more reducing equivalents than can be oxidized in the subsequent synthesis of isoleucine (Fig. 7A). The optimal flux solutions for *Rs. rubrum* strains grown on [1,4-^{13}C]fumarate estimated that the WT strain used the reductive pathway to make 72% of the isoleucine whereas 100% of isoleucine was made by the reductive pathway in the ΔCalvin mutant (Fig. 7A). Flux solutions from conditions using unlabeled malate and $Na^{13}CO_2$ were more skewed, indicating that 100% of isoleucine was made by the oxidative pathway in the WT strain whereas 100% of isoleucine was made by the reductive pathway in the ΔCalvin mutant (Fig. 7A). It is possible that the abundance of CO_2 in the malate + $Na^{13}CO_2$ condition alleviated the need for reductive isoleucine synthesis in the WT strain, for example, by stimulating Calvin cycle flux. Overall, our ^{13}C-MFA results suggest a role for reductive isoleucine synthesis in maintaining electron balance, especially when Calvin cycle activity is absent, as in the ΔCalvin mutant, or is limited by available CO_2.

298 To assess whether the reductive isoleucine pathway was essential for electron balance in
299 the absence of Calvin cycle activity, we deleted *ilvA*, encoding threonine dehydratase, in WT and
300 ΔPRK mutant backgrounds to prevent isoleucine synthesis via the reductive pathway. We also
301 grew WT and ΔCalvin *Rs. rubrum* strains in the presence of isoleucine, which has the potential
302 to inhibit both isoleucine synthesis pathways if they are regulated in *Rs. rubrum* as they are in *E.*
303 *coli* (28) and *Leptospira interrogans* (29). Neither deleting *ilvA* (Fig. 7B) nor adding isoleucine
304 to the growth medium (Fig. 7C) had a major effect on the growth trends of either the WT or the
305 Calvin cycle mutants. Thus, while the ^{13}C labeling patterns suggest that the flux through the two
306 isoleucine synthesis pathways is influenced by the need to maintain electron balance, the
307 reductive pathway is not essential for electron balance in *Rs. rubrum* Calvin cycle mutants.
308
309 **Sulfide production does not participate in electron balance in *Rs. rubrum*.** In addition to the
310 reverse TCA cycle flux suggested by the ^{13}C-labeling patterns, we also considered whether
311 pathways separate from carbon metabolism and H_2 production could contribute to electron
312 balance. Reduction of sulfate to sulfide by a spontaneous mutant of *Rb. sphaeroides* was
313 previously implicated as an alternative electron balancing mechanism (30). However, we did not
314 detect any sulfide in either WT or ΔCalvin mutant cultures using lead acetate strips (Fig. 8).
315
316 **Conclusion.** Overall, our data support previous results from our own group (8) and others (13)
317 that *Rs. rubrum* can maintain electron balance during photoheterotrophic growth on relatively
318 oxidized substrates without the Calvin cycle, H_2 production, or access to alternative electron
319 acceptors. While we consider it prudent to keep an open mind towards the possibility of an
320 additional reductive pathway, our results suggest that a *Rs. rubrum* Calvin cycle mutant can

maintain electron balance during phototrophic growth on malate and fumarate by using different biosynthetic pathways. The relatively static nature of biomass composition for a given growth condition places constraints on the extent to which different biosynthetic pathways can be employed to achieve electron balance, and thus likely explains why a *Rs. rubrum* Calvin cycle mutant cannot grow with succinate, which has only two more electrons than malate or fumarate (8). Our flux estimates suggest that electron balance through biosynthetic pathways in a *Rs. rubrum* Calvin cycle mutant is possible (Fig. 1C) and that alternative reductive pathways for synthesizing certain amino acids likely participate in electron balance, specifically, (i) the coupling of reverse TCA cycle flux to the synthesis of amino acids derived from αKG, and (ii) the use of a reductive pathway instead of an oxidative pathway for isoleucine synthesis. It is also possible that other biosynthetic pathways that would not be detected by our approach, such as altered fatty acid composition, could also offer limited flexibility to contribute to electron balance. Overall, our results highlight that while electron balance is a common challenge for all PNSB during photoheterotrophic growth, the strategies that come into play to address the challenge can differ between PNSB, with *Rs. rubrum* having electron-balancing mechanisms that others do not.

Methods.

Strains and growth conditions. *Rs. rubrum* strains ΔCalvin (UR2557, Δ*cbbM::*Gm^R Δ*cbbP*::Km^R (13)) and ΔPRK (UR2565, Δ*cbbP*::Km^R (13)) were derived from type-strain UR2 (32). *Rp. palustris* strains CGA676 (NifA*, (10)) and CGA4011 (NifA*, Δ*cbbLS*, Δ*cbbM*, Δ*cbbP*::Km^R (8)) were derived from type-strain CGA009. *Bacillus subtilis* 3610 (33) and *Escherichia coli* strains NEB10β (New England Biolabs) and WM3064 were cultured aerobically on LB agar or in LB broth. WM3064 is a diaminopimelic acid (DAP) auxotroph and

345 was thus supplemented with 0.6 mM DAP (W. Metcalf, unpublished data). *E. coli* strains were
346 stored in growth medium with 25% glycerol at -80°C. Other cultures were revived from 10%
347 DMSO (*Rs. rubrum*) or 25% glycerol (*Rp. palustris*) frozen stocks by streaking for single
348 colonies on photosynthetic medium (PM) agar (34) supplemented with 10 mM disodium
349 succinate and 0.1% yeast extract without antibiotics for *Rs. rubrum* and *Rp. palustris*. Colonies
350 were then used to inoculate 3 ml aerobic starter cultures of PM (*Rp. palustris*) or MA medium
351 (*Rs. rubrum*) (8), each with 10 mM succinate. Aerobic starter cultures were grown at 30°C with
352 shaking at 150 rpm. A 0.1 ml inoculum from stationary phase aerobic starter cultures was then
353 transferred to 10 ml anaerobic PM (*Rp. palustris*) or MA (*Rs. rubrum*) supplemented with 10
354 mM of an organic substrate as indicated in 28-ml anaerobic test tubes sealed with rubber
355 stoppers under an argon headspace, as described (8). Where indicated, media was supplemented
356 with specific amino acids at 20 mg/L each prior to inoculation. Antibiotics were not used in
357 comparative growth experiments or ^{13}C-labeling experiments but were otherwise added to media
358 where appropriate. Gentamycin and kanamycin were used at 100 µg/ml each for *Rp. palustris*
359 and at 10 µg/ml each for *Rs. rubrum.* Gentamycin was used at 15 µg/ml for *E. coli*.
360 **Analytical techniques.** Cell density was assayed by optical density (OD_{660}) using a Genesys 20
361 visible spectrophotometer (Thermo-Fisher, Pittsburgh, PA). Specific growth rates were
362 determined using measurements with values between 0.1 – 0.8 OD_{660}, where a linear
363 relationship between cell density and OD_{660} was maintained. H_2 was sampled from culture
364 headspace using a gas-tight syringe and analyzed using a Shimadzu GC-2014 gas chromatograph
365 as described (35). Organic acid levels in culture supernatants were determined by HPLC
366 (Shimadzu) as described (36). Sulfide was detected using lead acetate strips suspended above the
367 cultures. Strips were removed and photographed once cultures reached stationary phase (31).

368 ***Rs. rubrum* biomass composition.** Measurements were performed for the WT strain (UR2) and
369 the ΔCalvin mutant (UR2557) grown in MA medium. Culture samples were taken between 0.08
370 and 0.85 OD_{660} and measured using plastic cuvettes with a 1-cm path length. DCWs were
371 determined as described (37) by filtering 30 mL of culture through preweighed 0.22-μm HA
372 filters (Millipore) and then drying overnight at 80 °C. Protein was quantified using a
373 bicinchoninic acid assay (Pierce) as described (10). Amino acid composition was determined
374 using a Hitachi L-8800 amino acid analyzer at the University of California, Davis Molecular
375 Structure Facility. The polyhydroxybutyrate content was previously found to be below the
376 detection limit (8). Since protein accounted for 75% of the DCW, other major macromolecules
377 were assumed to make up the same proportions of the remaining DCW not accounted for in
378 protein as found in *Rp. palustris* and with the same monomeric composition. Biomass
379 compositions for each strain were combined since the slopes for linear regression of DCW/L vs
380 OD_{660} (400 ± 40 mg/L/ OD_{660}) and protein vs. DCW (75 ± 4% of DCW) were both found to be
381 statistically similar (Fig. S1; $p > 0.1$, determined using the linear regression analysis function in
382 Graphpad Prism 6.0h).
383 **^{13}C-labeling experiments and metabolic flux analysis.** Three or four biological replicates of
384 each strain were inoculated from unlabeled starter cultures into medium containing the indicated
385 ^{13}C-labeled substrate, provided at 100%. Cultures were harvested in exponential phase between
386 0.2 – 0.7 OD_{660} as described previously (10). Amino acids were obtained from the cell pellets by
387 hydrolysis in 6 N HCl, derivatized, and then MIDs determined using gas chromatography-mass
388 spectrometry (GC-MS) as described (37). GC-MS analysis was performed at the Indiana
389 University Mass Spectrometry Facility. MIDs were corrected for natural abundances of all atoms
390 except for carbons in amino acid backbones using IsoCor software (38). Corrected amino acid

391 mass isotopomer distributions and flux measurements (i.e., excreted malate and fluxes derived
392 from biomass composition (Table S2)) were used with a metabolic model mapping the carbon
393 atom transitions through *Rs. rubrum* central metabolism (Table S4) using the software suite
394 13CFLUX2 (19). Our *Rs. rubrum* model includes the TCA cycle, gluconeogenesis/glycolysis,
395 the Calvin cycle, the pentose phosphate pathway, and the ethylmalonyl-CoA pathway (Table
396 S4). Redox models that required that the sum of fluxes through reduction reactions equaled the
397 sum of fluxes through oxidation reactions used the following constraint (wherein biosynthetic
398 fluxes include those to EQPR):
399
400 WT: ECP1 + GNG2 + vIleT*5 + vIle_alt + 1.264 (biosynthetic NADPH oxidation) - 0.395
401 (biosynthetic NAD^+ reduction) - oppp - vPyrDH - vME - MalDH - SDH - aKGDH1 - aKGDH2 -
402 IDH = 0
403 ΔCalvin: ECP1 + GNG2 + vIleT*5 + vIle_alt + 0.753 (biosynthetic NADPH oxidation) - 0.235
404 (biosynthetic NAD^+ reduction) - oppp - vPyrDH - vME - MalDH - SDH - aKGDH1 - aKGDH2 -
405 IDH = 0
406
407 For each condition or model variation tested, at least 100 different arrangements of starting free
408 parameter values was chosen at random using the 13CFLUX2 program, multifit. An optimal
409 solution was selected based on that which has the lowest sum of squared residuals between
410 simulated and measured data sets of MIDs and biosynthetic and extracellular fluxes. Standard
411 deviations for flux values were determined using the 13CFLUX2 linearized statistical analysis
412 program, fwdsim.

413 ***Rs. rubrum* strain construction.** To create an in-frame deletion of Rru_A2721 (αKG synthase
414 α-subunit), the region upstream Rru_A2721 was amplified using primers BL50
415 (gacttctagactataacgatctggccgattggc) and BL524 (gactggtacccgtcatcatccgtctttcagagaag) and the
416 region downstream was amplified using primers BL525 (gactggtacccagggagagtgatcatggatacg)
417 and BL504 (gacttctagaactgggcttcgatttcggtgaa). The resulting PCR products were digested using
418 KpnI, ligated together, and then the ligation reaction was used as template for a second round of
419 PCR using primers BL501 and BL504. The resulting PCR product was purified, digested with
420 XbaI, and then ligated into XbaI-digested pJQ200SK (39). To create an in-frame deletion of
421 Rru_A2877 (*ilvA*, threonine deaminase), the upstream region was amplified using BL646
422 (gctggagctccaccgtgactccgtctggccccaag) and BL635 (tccccggcggtcatcgtccgccctcc) and the
423 downstream region was amplified using BL636 (cgatgaccgccggggattagggcaaatc) and BL647
424 (attcctgcagcccggcgtcgattacaccggcctc). The upstream and downstream PCR products were mixed
425 with pJQ200SK, which was PCR-linearized using BL644 (cggtggagctccagcttttg) and BL645
426 (ccgggctgcaggaattcg), and then assembled by Gibson Assembly (NEB). Ligation and Gibson
427 reactions were transformed into *E. coli* NEB10β (New England Biolabs) and transformants
428 verified by PCR and sequencing. Vectors were then introduced into electrocompetent *E.*
429 *coli* WM3064.
430 Vectors containing deletion constructs were transferred to *Rs. rubrum* strains by conjugation
431 with WM3064 on PM agar with yeast extract, succinate, and DAP. Mating patches were streaked
432 for single recombinants on PM agar with yeast extract, succinate, and Gm. Colonies were then
433 grown in liquid media without Gm to allow for a second recombination event. Cultures were
434 plated to PM agar with yeast extract, succinate, and 10% sucrose, screened for Gm sensitivity,
435 and then Gm-sensitive colonies were screened by PCR for the desired mutations.

Acknowledgements. This work was funded by the Indiana University College of Arts and Sciences. We thank GC Gordon for contributions to preliminary studies and JA Karty for GCMS training and advice.

References

1. Erb TJ. 2011. Carboxylases in natural and synthetic microbial pathways. Appl Environ Microbiol 77:8466-8477.
2. Muller FM. 1933. On the metabolism of the purple sulphur bacteria in orgainic media. Arch Microbiol 4:131-166.
3. Hallenbeck PL, Lerchen R, Hessler P, Kaplan S. 1990. Roles of CfxA, CfxB, and external electron acceptors in regulation of ribulose 1,5-bisphosphate carboxylase/oxygenase expression in *Rhodobacter sphaeroides*. J Bacteriol 172:1736-1748.
4. Hallenbeck PL, Lerchen R, Hessler P, Kaplan S. 1990. Phosphoribulokinase activity and regulation of CO_2 fixation critical for photosynthetic growth of *Rhodobacter sphaeroides*. J Bacteriol 172:1749-1761.
5. Paoli GC, Vichivanives P, Tabita FR. 1998. Physiological control and regulation of the *Rhodobacter capsulatus cbb* operons. J Bacteriol 180:4258-4269.
6. Falcone DL, Tabita FR. 1991. Expression of endogenous and foreign ribulose 1,5-bisphosphate carboxylase-oxygenase (RubisCO) genes in a RubisCO deletion mutant of *Rhodobacter sphaeroides*. J Bacteriol 173:2099-2108.
7. McCully AL, McKinlay JB. 2016. Disrupting Calvin cycle phosphoribulokinase activity in *Rhodopseudomonas palustris* increases the H_2 yield and specific production rate proportionately. Int J Hydrogen Energy 41:4143-4149.
8. Gordon GC, McKinlay JB. 2014. Calvin cycle mutants of photoheterotrophic purple nonsulfur bacteria fail to grow due to an electron imbalance rather than toxic metabolite accumulation. J Bacteriol 196:1231-1237.
9. McKinlay JB, Harwood CS. 2011. Calvin cycle flux, pathway constraints, and substrate oxidation state together determine the H_2 biofuel yield in photoheterotrophic bacteria. mBio 2: e01620-17.
10. McKinlay JB, Harwood CS. 2010. Carbon dioxide fixation as a central redox cofactor recycling mechanism in bacteria. Proc Natl Acad Sci U S A 107:11669-11675.
11. Farmer RM, Laguna R, Panescu J, McCoy A, Logsdon B, Zianni M, Moskvin OV, Gomelsky M, Tabita FR. 2014. Altered residues in key proteins influence the expression and activity of the nitrogenase complex in an adaptive CO_2 fixation-deficient mutant strain *of Rhodobacter sphaeroides*. Microbiology 160:198-208.
12. Öztürk Y, Gökçe A, Peksel B, Gürgan M, Özgür E, Gündüz U, Eroğlu I, Yücel M. 2012. Hydrogen production properties of *Rhodobacter capsulatus* with genetically modified redox balancing pathways. Int J Hydrogen Energy 37:2014–2020.
13. Wang D, Zhang Y, Pohlmann EL, Li J, Roberts GP. 2011. The poor growth of *Rhodospirillum rubrum* mutants lacking RubisCO is due to the accumulation of ribulose-1,5-bisphosphate. J Bacteriol 193:3293-3303.

14. Hädicke O, Grammel H, Klamt S. 2011. Metabolic network modeling of redox balancing and biohydrogen production in purple nonsulfur bacteria. BMC Syst Biol 5:150.
15. Wang X, Modak HV, Tabita FR. 1993. Photolithoautotrophic growth and control of CO_2 fixation in *Rhodobacter sphaeroides* and *Rhodospirillum rubrum* in the absence of ribulose bisphosphate carboxylase-oxygenase. J Bacteriol 175:7109-7114.
16. De Meur Q, Deutschbauer A, Koch M, Wattiez R, Leroy B. 2018. Genetic plasticity and ethylmalonyl coenzyme A pathway during acetate assimilation in *Rhodospirillum rubrum* S1H under photoheterotrophic conditions. Appl Environ Microbiol 84: e02038-17.
17. Buchanan BB, Evans MC, Arnon DI. 1967. Ferredoxin-dependent carbon assimilation in *Rhodospirillum rubrum*. Arch Mikrobiol 59:32-40.
18. Buescher JM, Antoniewicz MR, Boros LG, Burgess SC, Brunengraber H, Clish CB, DeBerardinis RJ, Feron O, Frezza C, Ghesquiere B, Gottlieb E, Hiller K, Jones RG, Kamphorst JJ, Kibbey RG, Kimmelman AC, Locasale JW, Lunt SY, Maddocks OD, Malloy C, Metallo CM, Meuillet EJ, Munger J, Noh K, Rabinowitz JD, Ralser M, Sauer U, Stephanopoulos G, St-Pierre J, Tennant DA, Wittmann C, Vander Heiden MG, Vazquez A, Vousden K, Young JD, Zamboni N, Fendt SM. 2015. A roadmap for interpreting ^{13}C metabolite labeling patterns from cells. Curr Opin Biotechnol 34:189-201.
19. Weitzel M, Noh K, Dalman T, Niedenfuhr S, Stute B, Wiechert W. 2013. 13CFLUX2-high-performance software suite for ^{13}C-metabolic flux analysis. Bioinformatics 29:143-145.
20. Joshi HM, Tabita FR. 2000. Induction of carbon monoxide dehydrogenase to facilitate redox balancing in a ribulose bisphosphate carboxylase/oxygenase-deficient mutant strain of *Rhodospirillum rubrum*. Arch Microbiol 173:193-199.
21. Ragsdale SW, Pierce E. 2008. Acetogenesis and the Wood-Ljungdahl pathway of CO_2 fixation. Biochim Biophys Acta 1784:1873-1898.
22. Bonam D, Ludden PW. 1987. Purification and characterization of carbon monoxide dehydrogenase, a nickel, zinc, iron-sulfur protein, from *Rhodospirillum rubrum*. J Biol Chem 262:2980-2987.
23. Perez-Arellano I, Rubio V, Cervera J. 2006. Mapping active site residues in glutamate-5-kinase. The substrate glutamate and the feed-back inhibitor proline bind at overlapping sites. FEBS Lett 580:6247-6253.
24. Caspi R, Billington R, Fulcher CA, Keseler IM, Kothari A, Krummenacker M, Latendresse M, Midford PE, Ong Q, Ong WK, Paley S, Subhraveti P, Karp PD. 2018. The MetaCyc database of metabolic pathways and enzymes. Nucleic Acids Res 46:D633-D639.
25. Leisinger T, Haas D. 1975. N-Acetylglutamate synthase of *Escherichia coli* regulation of synthesis and activity by arginine. J Biol Chem 250:1690-1693.
26. Jiang P, Peliska JA, Ninfa AJ. 1998. The regulation of *Escherichia coli* glutamine synthetase revisited: role of 2-ketoglutarate in the regulation of glutamine synthetase adenylylation state. Biochemistry 37:12802-12810.
27. Miller RE, Stadtman ER. 1972. Glutamate synthase from *Escherichia coli*. An iron-sulfide flavoprotein. J Biol Chem 247:7407-7419.
28. Eisenstein E, Yu HD, Schwarz FP. 1994. Cooperative binding of the feedback modifiers isoleucine and valine to biosynthetic threonine deaminase from *Escherichia coli*. J Biol Chem 269:29423-29429.
29. Xu H, Zhang Y, Guo X, Ren S, Staempfli AA, Chiao J, Jiang W, Zhao G. 2004. Isoleucine biosynthesis in *Leptospira interrogans* serotype lai strain 56601 proceeds via a threonine-independent pathway. J Bacteriol 186:5400-5409.

30. Rizk ML, Laguna R, Smith KM, Tabita FR, Liao JC. 2011. Redox homeostasis phenotypes in RubisCO-deficient *Rhodobacter sphaeroides* via ensemble modeling. Biotechnol Prog 27:15-22.
31. Xia Y, Lu C, Hou N, Xin Y, Liu J, Liu H, Xun L. 2017. Sulfide production and oxidation by heterotrophic bacteria under aerobic conditions. ISME J 11:2754-2766.
32. Fitzmaurice WP, Saari LL, Lowery RG, Ludden PW, Roberts GP. 1989. Genes coding for the reversible ADP-ribosylation system of dinitrogenase reductase from *Rhodospirillum rubrum*. Mol Gen Genet 218:340-347.
33. Kearns DB, Losick R. 2003. Swarming motility in undomesticated *Bacillus subtilis*. Mol Microbiol 49:581-590.
34. Kim M, Harwood CS. 1991. Regulation of benzoate-CoA ligase in *Rhodopseudomonas palustris*. FEMS Microbiol Lett 83:199-203.
35. Huang JJ, Heiniger EK, McKinlay JB, Harwood CS. 2010. Production of hydrogen gas from light and the inorganic electron donor thiosulfate by *Rhodopseudomonas palustris*. Appl Environ Microbiol 76:7717-7722.
36. McKinlay JB, Zeikus JG, Vieille C. 2005. Insights into *Actinobacillus succinogenes* fermentative metabolism in a chemically defined growth medium. Appl Environ Microbiol 71:6651-6656.
37. McKinlay JB, Shachar-Hill Y, Zeikus JG, Vieille C. 2007. Determining *Actinobacillus succinogenes* metabolic pathways and fluxes by NMR and GC-MS analyses of ^{13}C-labeled metabolic product isotopomers. Metab Eng 9:177-192.
38. Millard P, Letisse F, Sokol S, Portais JC. 2012. IsoCor: correcting MS data in isotope labeling experiments. Bioinformatics 28:1294-1296.
39. Quandt J, Hynes MF. 1993. Versatile suicide vectors which allow direct selection for gene replacement in gram-negative bacteria. Gene 127:15-21.

548 **Figures and legends**

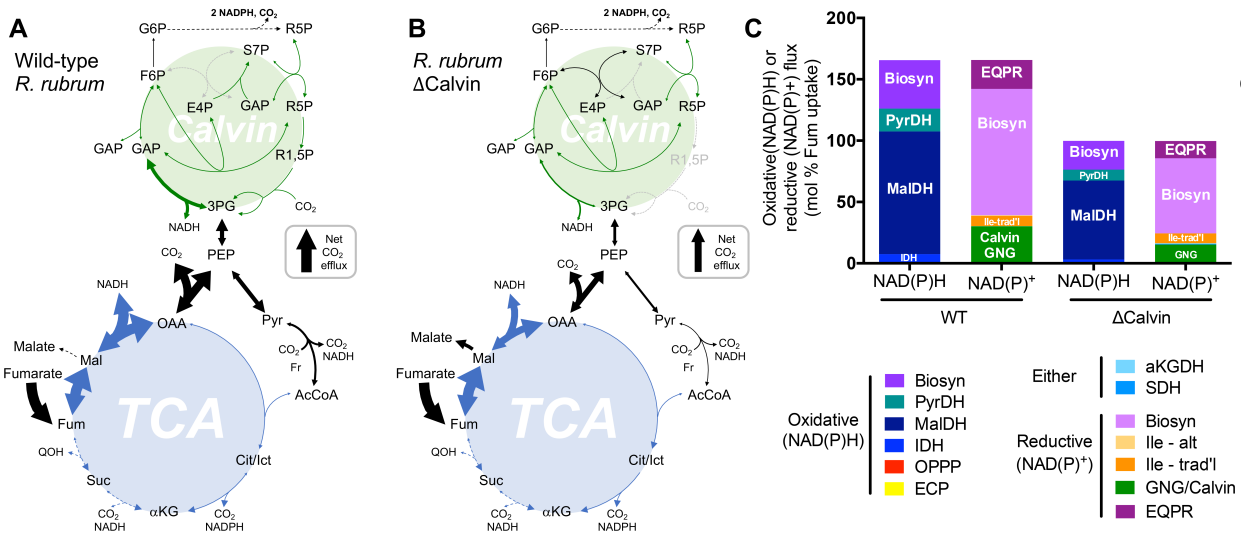

549

550 **Fig. 1.** Redox-constrained flux models suggest reverse TCA cycle flux from fumarate to αKG for
551 WT *Rs. rubrum* (UR2) (A) and the ΔCalvin mutant (UR2557) (B) grown phototrophically on
552 malate. The ethylmalonyl-CoA pathway was estimated to carry negligible flux and is not shown
553 for simplicity. Flux magnitudes are indicated by arrow thickness. Net flux direction is indicated
554 by an enlarged arrowhead. Fluxes that have a value of less than 1 mol % of the fumarate uptake
555 rate are shown as dashed arrows. (C) Comparison of fluxes through redox reactions. NAD(P)H
556 columns refer to those reactions that reduce electron carriers (oxidative pathways), whereas
557 $NAD(P)^+$ columns refer to those reactions that oxidize electron carriers (reductive pathways).
558 Biosyn, biosynthesis; PyrDH, pyruvate dehydrogenase; MalDH, malate dehydrogenase; IDH,
559 isocitrate dehydrogenase; OPPP, oxidative pentose phosphate pathway; ECP, ethylmalonyl-CoA
560 pathway; aKGDH, αKG dehydrogenase/synthase; SDH, succinate dehydrogenase; Ile – alt,
561 isoleucine synthesis from pyruvate and AcCoA; Ile – trad'l, isoleucine synthesis from pyruvate
562 and oxaloacetate; GNG/Calvin, glyceraldehyde-3-phosphate dehydrogenase in either
563 gluconeogenesis or the Calvin cycle; EQPR, synthesis of Glu, Gln, Pro, and Arg. (A-C) All
564 fluxes are normalized to the fumarate uptake rate for each strain. Absolute flux values were 1.73

565 ± 0.09 and 0.66 ± 0.16 mmol fumarate / g DCW/ h ± SD, for the WT and ΔCalvin mutant,

566 respectively. All flux values are in Table S4.

567

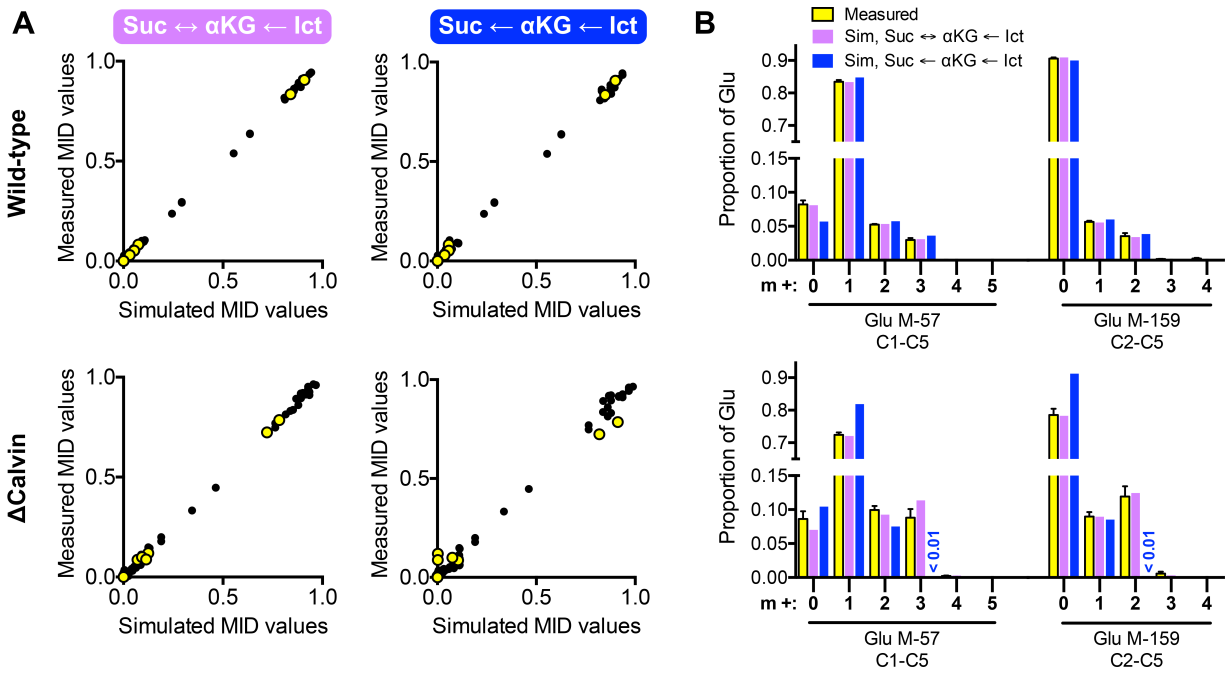

568

569 **Fig. 2.** Reverse TCA cycle flux is required to explain Glu MIDs in the *Rs. rubrum* ΔCalvin

570 mutant. (A, B) Top, WT *Rs. rubrum* (UR2); bottom, *Rs. rubrum* ΔCalvin (UR2557). **A.** Linear

571 regression of measured vs simulated MID values from the optimal flux solutions for strains

572 grown with [1,4-^{13}C]fumarate. Simulations used a flux model that either allowed (left) or did not

573 allow (right) for reversible flux between succinate (Suc) and αKG. Irreversible flux from

574 isocitrate (Ict) to αKG was assumed for all flux models. Yellow, Glu MIDs; black, MIDs for all

575 other examined amino acids. **B.** Comparison of measured and simulated (Sim) Glu MIDs from

576 panel A. Error bars, SD; n=4.

577

578

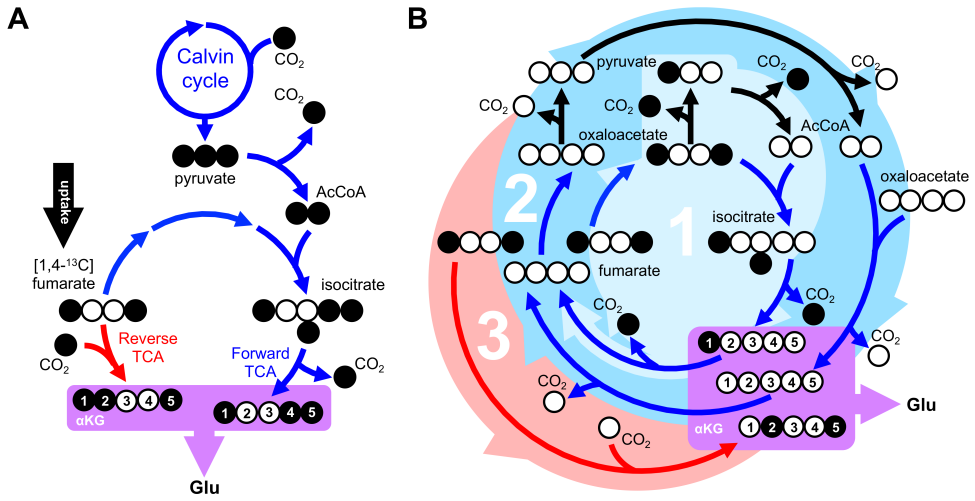

579

580 **Fig. 3.** Possible mechanisms leading to the production of triple-labeled glutamate (**A**) or lower

581 MW glutamate isotopomers (**B**) from [1,4-^{13}C]fumarate in *Rs. rubrum*. Note that double- and

582 triple-labeled glutamate are each expected to arise from reverse TCA cycle activity, especially in

583 a ΔCalvin mutant. Black, ^{13}C; white, ^{12}C.

584

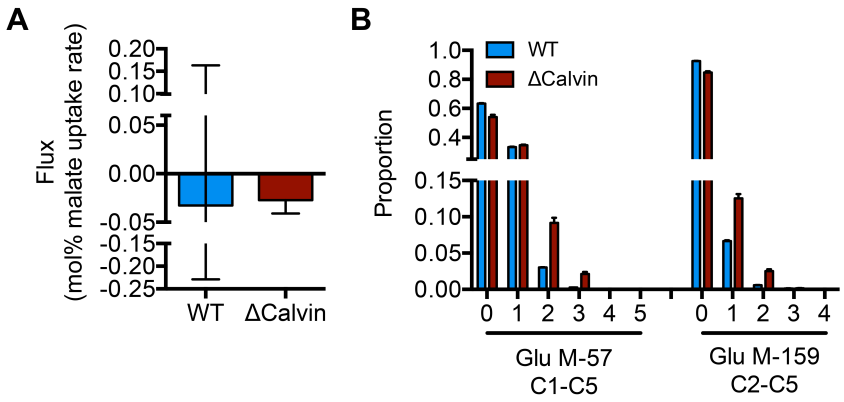

585

586 **Fig. 4.** Flux estimates from MIDs generated during phototrophic growth on unlabeled malate and

587 $NaH^{13}CO_3$ suggest reverse TCA cycle flux from fumarate to αKG in the *Rs. rubrum* ΔCalvin

588 mutant. (A) Estimate flux through αKG dehydrogenase/synthase (positive: αKG → succinate;

589 negative: succinate → αKG) from the optimal flux solutions. (B) Comparison of measured Glu

590 MIDs from the WT strain (UR2) and the ΔCalvin mutant (UR2557). Error bars, SD; n=3.

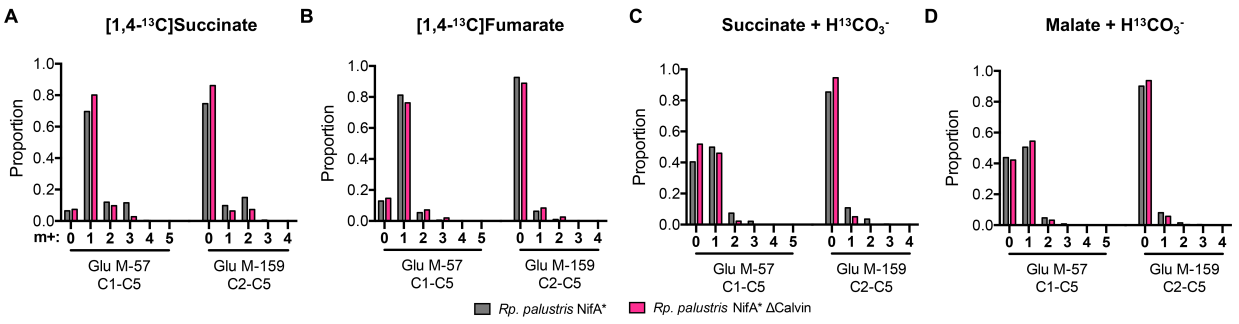

Fig. 5. Glu MIDs from *Rp. palustris* NifA* (CGA676) and a *Rp. palustris* NifA* Calvin cycle mutant (CGA4011) grown phototrophically on [1,4-^{13}C]succinate (A), [1,4-^{13}C]fumarate (B), succinate + NaH^{13}CO$_3$ (C), or malate + NaH^{13}CO$_3$ (D). CGA676 data from [1,4-^{13}C]succinate and [1,4-^{13}C]fumarate conditions were reported previously (9).

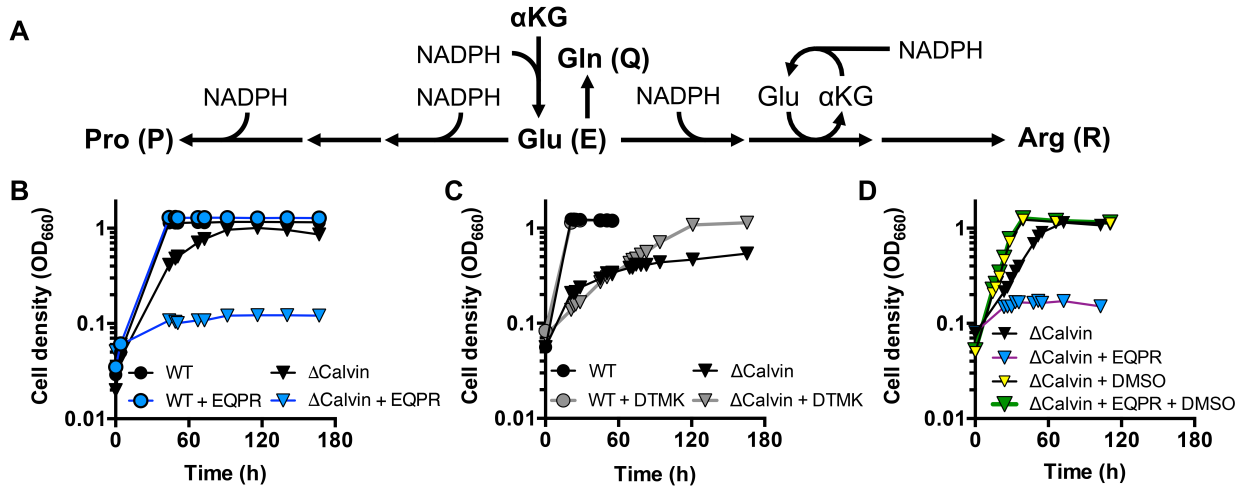

Fig. 6. αKG-derived amino acids represses phototrophic growth of the *Rs. rubrum* ΔCalvin mutant on malate. (A) Abbreviated pathway illustrating the redox reactions involved in the synthesis of the four amino acids synthesized from αKG-derived. (B-D) Growth curves for WT and the ΔCalvin mutant grown with either a mixture of glutamate, glutamine, proline, and arginine (EQPR) (B) with or without DMSO (D) or with a mixture of aspartate, threonine, methione, and lysine (C; DTMK).

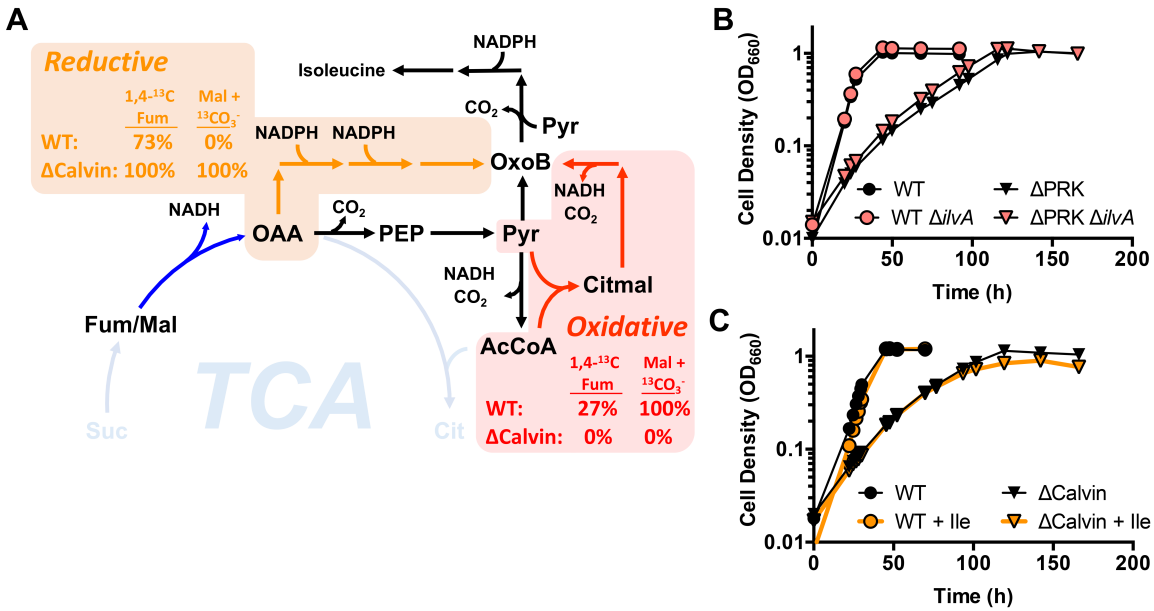

605

606 **Fig. 7. *Rs. rubrum* Calvin cycle mutants use a non-essential reductive isoleucine synthesis**

607 **pathway.** (A) Estimated fluxes as a percent of total isoleucine synthesis for the reductive

608 (orange) and oxidative (red) isoleucine synthesis pathways for the WT and ΔCalvin strains

609 during growth on either [1,4-^{13}C]fumarate or malate with NaH^{13}CO$_3$. (B) Effect of deleting the

610 *ilvA*, encoding threonine deaminase in the reductive isoleucine synthesis pathway, on growth

611 trends in WT and ΔPRK backgrounds. (C) Effect of adding isoleucine on the growth trends of

612 WT and ΔCalvin strains.

613

614

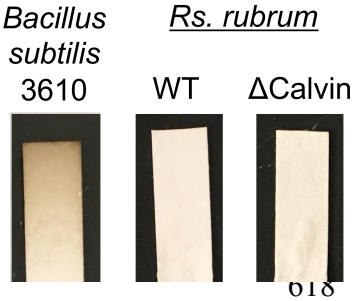

618

Fig. 8. *Rs. rubrum* cultures test negative for sulfide production using lead acetate strips. Strips darken when exposed to sulfide. An aerobic culture of *Bacillus subtilis* 3610 grown in LB medium was used as a positive control for sulfide production (31). Similar trends were observed for 2 other biological replicates.

619

Supplementary figures and legends

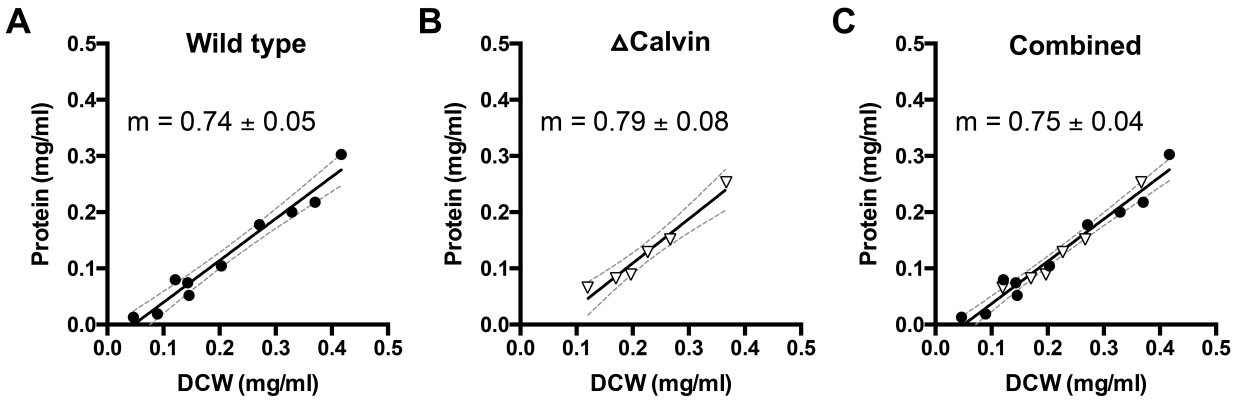

Fig S1. Protein makes up 75% of *Rs. rubrum* DCW based on linear regression. WT (UR2; A) and the ΔCalvin mutant (UR2557; B) were grown in MA medium with 10 mM disodium fumarate. The solid line indicates the averaged slope and the dashed lines show 95% CI. There was no statistical difference between the slopes for the WT and ΔCalvin plots according to a linear regression analysis by Graphpad Prism 6.0h. Therefore the combined data were used to determine the *Rs. rubrum* protein content (C).

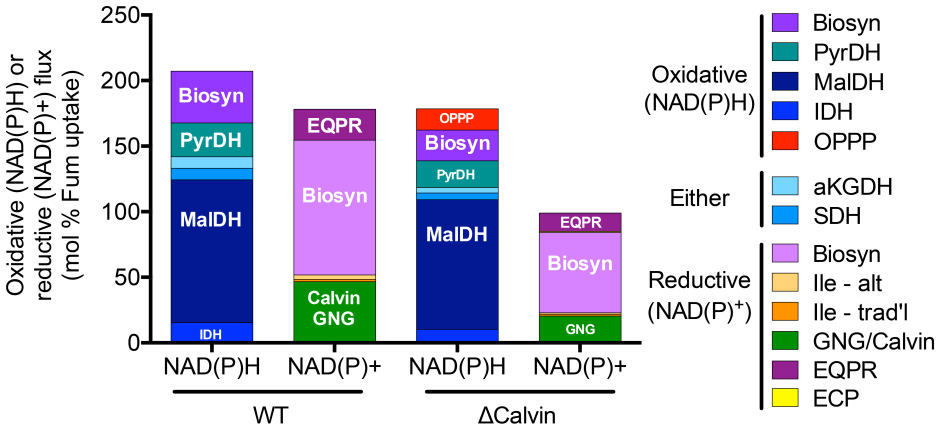

Fig. S2. Unconstrained flux solutions for WT *Rs. rubrum* (UR2; A) and the ΔCalvin mutant (UR2557; B) grown phototrophically on [1,4-^{13}C]fumarate do not satisfy electron balance. Fluxes through reactions that either reduce electron carriers (oxidative pathways; NAD(P)H) or oxidize electron carriers (reductive pathways; $NAD(P)^+$) are shown. A complete set of flux values is available in Table S4.

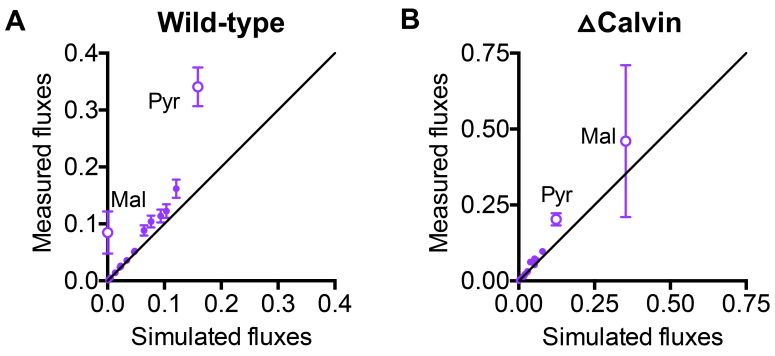

Fig. S3 *Rs. rubrum* flux models fail to fully explain biomass composition. Flux values are mole % of fumarate uptake rate. Each symbol represents either malate excretion (Mal) or the total flux from a central metabolite needed to make components of biomass according to Table S2 (e.g., the flux from pyruvate [Pyr] needed to make fatty acids, amino acids, etc.). Error bars, SD. SD for malate was based on experimental measurements. SD for other biomass fluxes was assumed to be 10% of the flux value.